Available online at www.sciencedirect.com
SCIENCE DIRECT®
Journal of Catalysis 236 (2005) 129–138
JOURNAL OF CATALYSIS
www.elsevier.com/locate/jcat

First-principles based kinetic model for the hydrogenation of toluene

Mark Saeys [a,b], Marie-Françoise Reyniers [a,*], Joris W. Thybaut [a], Matthew Neurock [c], Guy B. Marin [a]

[a] *Laboratorium voor Petrochemische Techniek, Ghent University, Krijgslaan 281(S5), B-9000 Gent, Belgium*
[b] *Department of Chemical and Biomolecular Engineering, National University of Singapore, 4 Engineering Drive 4, Singapore 117576*
[c] *Department of Chemical Engineering, University of Virginia, 102 Engineers' Way, Charlottesville, VA 22904-4741, USA*

Received 31 May 2005; revised 15 September 2005; accepted 17 September 2005

Available online 20 October 2005

Abstract

A fundamental kinetic model for the hydrogenation of toluene over platinum has been constructed, based on detailed first-principles density functional theory calculations for the hydrogenation of benzene over Pt(111). A Langmuir–Hinshelwood–Hougen–Watson (LHHW) kinetic model was derived based on an ab initio reaction path analysis [M. Saeys, M.-F. Reyniers, M. Neurock, G.B. Marin, J. Phys. Chem. B 109 (2005) 2064], enabling easy interpretation and evaluation of the parameters appearing in the rate equation. The activation energy, adsorption, and reaction enthalpies in the model were obtained from the first-principles calculations. The pre-exponential factors were calculated from statistical mechanics, using assumptions derived from the first-principles results. The coverage-dependent hydrogen chemisorption enthalpy was optimized to accurately model lab-scale experimental data for the gas phase hydrogenation of toluene over a 0.5 wt% Pt/ZSM-22 catalyst. The resulting hydrogen chemisorption enthalpy of -54.0 ± 1.0 kJ/mol falls between the high and low coverage values, consistent with a simulated average hydrogen surface coverage of 61%. The LHHW model based on the ab initio calculations captures the main trends in the reaction rates. The reaction model predicts reaction orders for the inlet partial pressure of hydrogen and toluene ranging from 1.6 to 2.2 and from -0.4 to 0.7, respectively. This is in reasonable agreement with experimental values, which range from 1.3 to 1.8 and from -0.3 to 0.3, respectively.

Keywords: Hydrogenation; First-principles modeling; Kinetic modeling; Benzene; Toluene

1. Introduction

The development and optimization of chemical processes requires accurate reaction models that are applicable over a wide range of process conditions. Computer simulation has become invaluable to complement experimental studies for achieving these goals. Models to describe industrial chemical processes are based on mathematical reactor models that account for both the chemical reactions and the physical transport phenomena that occur on the industrial scale. Traditionally, most reaction models are based on the interpolation of experimental data or consist of power law models that describe the global kinetics and are devoid of the elementary-step kinetics. This can limit their applicability to a restricted range of process conditions, as well as their accuracy. Microkinetic models constructed from the fundamental kinetics of the elementary reaction steps offer the ability to cover a broader range of process conditions, along with improved accuracy. The development of green processes that minimize energy use and waste production necessitates fully accounting for the fate of all intermediates formed and thus requires more detailed reaction kinetic models, taking into account the molecular transformations occurring on the catalyst surface.

For many years, the construction of kinetic models for industrial catalytic reactions has been based largely on the combination of a large empirical database and the qualitative concepts of chemical reactivity. The ever-increasing computational resources and the continuous improvement in quantum chemistry methods and software provide valuable tools for the kinetic modeling of heterogeneous catalytic reactions. Carefully chosen quantum chemical methods can provide qualitative and/or quantitative insight into the details of catalytic processes [2]. In a number of cases, reliable kinetic models have been con-

* Corresponding author. Fax: +32 9 264 49 99.
E-mail addresses: mariefrancoise.reyniers@ugent.be (M.-F. Reyniers), guy.marin@ugent.be (G.B. Marin).

0021-9517/$ – see front matter
doi:10.1016/j.jcat.2005.09.019

structed from first principles. Examples are the hydrogenation of ethene [3,4], the hydrogenolysis of ethane [5], ammonia synthesis [6], and the selective oxidation of ethene [7].

In this paper we explore the capabilities of these computational tools for developing reaction models for industrially relevant systems composed of more complex reactants. The hydrogenation of aromatics over platinum was selected as a test case in view of its relevance in various industrial processes. The catalytic hydrogenation of aromatic compounds is an important reaction for the production of clean, high-quality fuels. Environmental concerns continue to impose ever-stricter limits on the aromatic content of fuels [8]. In addition, cyclohexane, a base chemical for the production of nylon 6 and nylon 66, is produced industrially via benzene hydrogenation. As compared with previously reported cases [3–7], aromatic hydrogenation is a somewhat more complex reaction, consisting of at least six sequential elementary hydrogenation steps. Moreover, the larger-sized aromatic molecules require a larger cluster or unit cell to accurately model the catalyst surface.

Numerous experimental kinetic studies on the hydrogenation of aromatics are available in the literature. These studies propose various reaction models in attempts to capture the laboratory data. Lin and Vannice [9] derived a model in which the addition of the first hydrogen atom to the aromatic ring was proposed as the rate-determining step (RDS). The concurrently formed H-deficient surface species was considered the most-abundant reaction intermediate (MARI). Others have selected the addition of the first H_2 molecule or the simultaneous addition of the first two H-atoms as rate-determining [10–13]. Models proposed by Lindfors et al. [13] and Van Meerten and Coenen [14] assume equal rate coefficients for all hydrogenation steps. The model derived by Chou and Vannice [15] considers a linear increase in activation energies and a linear decrease in activation entropies between the first and sixth hydrogen additions. Based on physicochemical arguments, Thybaut et al. [16] selected a model with equal reaction rate coefficients for the first four hydrogenations and competitive toluene and H adsorption. The fifth and sixth hydrogenation steps were assumed to be irreversible. Thybaut et al. [16] also demonstrated that, as a limiting case of their more general model, a kinetic model where the fourth hydrogenation is considered rate-determining can be obtained.

The adsorption and dehydrogenation of cyclic C_6 molecules on transition metals has also received considerable attention from both the surface science and theoretical communities. From these studies, a fairly consistent picture has emerged. Various investigators have combined data from spectroscopic and surface science studies with results from density functional theory (DFT) to gain a clear understanding of the adsorption of benzene on Pt(111), Pd(111), Rh(111), and Ni(111) [17,18] and of the adsorption of cyclohexadiene [19] and cyclohexene [20] on Pt(111). From these and other studies, it has become clear that DFT calculations provide reasonably accurate descriptions of the adsorption and dehydrogenation of unsaturated hydrocarbons on Pt(111), yielding adsorption and activation energies typically within 10 kJ/mol of experimental data.

Previously, we carried out an extensive set of ab initio calculations to obtain a detailed understanding of the mechanism of benzene hydrogenation to cyclohexane [1,17,20,21]. Similar to ethene hydrogenation [3], benzene hydrogenation was found to follow a Horiuti–Polanyi-type mechanism in which hydrogen atoms add sequentially to the adsorbed benzene molecule [21]. Benzene adsorbs at two different sites [17]: a hollow (30) site and a bridge (0) site, with low coverage adsorption energies of −71 and −102 kJ/mol, respectively. Ab initio DFT calculations were performed to analyze the reaction path for benzene hydrogenation to cyclohexane [1]. The DFT results were analyzed using fundamental concepts introduced by Boudart [22], that is, the concepts of catalytic cycle, RDS, and MARI. Out of all possible catalytic cycles, one dominant path was found along which the activation energy for every step is at least 18 kJ/mol lower than for any possible alternative elementary step that branches from the dominant path [1] (Fig. 1). The activation energies for the different steps along the dominant path

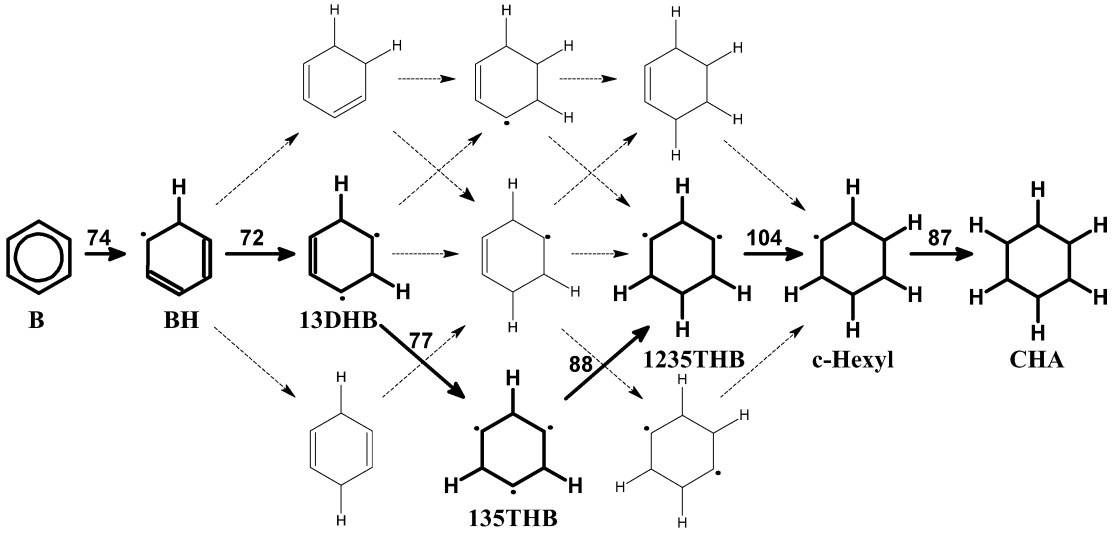

Fig. 1. Overview of the different reaction paths for benzene hydrogenation. The dominant reaction path is indicated in boldface. The hydrogenation activation energies (kJ/mol) for every step along the dominant reaction path are indicated.

are also reported in Fig. 1. The highest barrier, 104 kJ/mol, was calculated for step 5 forming cyclohexyl. This step can be considered "far from equilibrium" and thus rate-determining [1].

From the ab initio reaction path analysis, a detailed qualitative picture of benzene hydrogenation over Pt(111) has emerged. Based on this picture, we constructed a LHHW kinetic model for the hydrogenation of toluene over an industrial Pt catalyst. The kinetic and thermodynamic parameters in the model were derived from the ab initio calculations. To evaluate the accuracy of this approach, the predictions of the first-principles based kinetic model are validated by comparison with experimental data for the hydrogenation of toluene over a 0.5 wt% Pt/ZSM-22 catalyst [16].

Although the hydrogenation kinetics for toluene can be expected to differ slightly from those for benzene, trends can be expected to be comparable [9,23]. Considering the fairly simple main field approximations in the LHHW reaction model, perfect agreement with experimental data should indeed not be expected, yet the main trends should be reproduced.

2. Methods

2.1. Quantum chemical calculations

The optimal ab initio method to study benzene hydrogenation was found to be [17,21] relativistic DFT with the Becke–Perdew (BP86) functional (e.g., [24]) and a double-zeta Slater type orbitals (STO) basis set. The Pt(111) catalyst was modeled by a two-layer Pt_{22} cluster. A more detailed description of the computational procedure has been presented elsewhere [17].

The calculations were performed for a (111) surface, whereas the catalyst particles in the experiment are more or less spherical with an average diameter of 3 nm. The (111) surface was selected for the calculations because it is the closest-packed and the thermodynamically most stable facet. Hence it can be expected to dominate the fairly large catalyst particles. Moreover, hydrogenation is a structure insensitive reaction [1], and the data from the (111) surface should be applicable to other facets as well.

2.2. Experimental setup

Toluene hydrogenation was studied over ZSM-22 loaded with 0.5 wt% Pt. The preparation of the catalyst has been described elsewhere [16,26]. A Pt dispersion of 30% was measured [26], indicating that the Pt metal is present as particles with a diameter of 3 nm and is located on the external surface of the zeolite crystallites, because the crystal pores have a cross-section of only 0.45 × 0.55 nm [26]. The concentration of active sites, C_t, can be calculated from the dispersion and the catalyst loading and amounts to 0.8×10^{-2} mol kg_{cat}^{-1}. Because of the shape-selective character of the intracrystalline pores of the ZSM-22 zeolite, acid-catalyzed cracking and isomerization products were observed in only minor amounts. The absence of mass transport limitations in the intercrystalline pores was verified (Weisz moduli $\sim 10^{-2}$) [16]. Note that the intracrystalline diffusion limitations are not relevant, because hydrogenation occurs on the external crystallite surface [16].

Toluene was used as model component in the experimental work because its hydrogenated product, methylcyclohexane, has very limited isomerization possibilities, hence limiting possible side reactions. Although benzene hydrogenation was studied in the ab initio reaction path analysis and cyclohexane has even less isomerization possibilities, the use of benzene was rejected for an extended set of experiments because of its carcinogenic character.

Benzene rather than toluene was selected for the ab initio study because a large number of surface science studies on benzene adsorption are available, enabling validation of the theoretical procedures. Much less surface science data are available for toluene adsorption, and no experimental adsorption energies have been determined. Moreover, the high symmetry of benzene significantly reduces the complexity of the ab initio reaction path analysis.

Experiments were performed in a gas phase continuous stirred tank reactor (Berty [27] reactor). Nitrogen was used to vary the H_2 and toluene partial pressures under which reactant conversion was measurable and not transport-limited at the total pressures applied. Hydrogen (99.99%, $H_2O + O_2$ content < 10 ppm; L'Air Liquide) and toluene (99%; Acros) were used without further purification. Methane was used as an internal standard. The equipment has a stabilization time of about 1 h, after which a sample of the reactor effluent was taken and sent to a HP Series II 5890 gas chromatograph equipped with a 50-m RSL-150 column with a 0.25-μm poly(dimethylsiloxane) film.

To avoid catalyst deactivation, a 10 $mmol_{H_2}\ s^{-1}$ flow was sent through the reactor between experiments. A total of 42 experiments were carried out, varying the H_2 inlet partial pressure from 100 to 300 kPa, the toluene inlet partial pressure from 10 to 60 kPa, the temperature from 423 to 498 K, and the space velocity from 27 to 82 $kg_{cat}\ mol^{-1}\ s^{-1}$. Conversion ranged from 5 to 45%. The total pressure (i.e., including N_2) ranged from 1 to 3 MPa.

2.3. Parameter estimation

The activation and adsorption energies in the ab initio kinetic model were obtained from the first-principles calculations. Because the ab initio parameters were obtained from cluster DFT calculations, they correspond effectively to zero coverage values. However, the hydrogen adsorption enthalpy has been found to be strongly coverage-dependent [28]. At low coverage, a dissociative adsorption enthalpy from −60 to −90 kJ/mol has been reported, consistent with DFT results [21]. The adsorption enthalpy decreases dramatically with coverage to about −40 kJ/mol at monolayer coverage [28]. Because the hydrogen adsorption enthalpy is an important parameter in our kinetic model, this strong coverage dependence complicates a first-principles assessment of this parameter. To reproduce the experimental data, we therefore selected the hydrogen adsorption enthalpy to be the only adjustable parameter in the kinetic model. Other parameters are also likely coverage-dependent, but experimental data seem to indicate that the hollow site ben-

zene adsorption enthalpy is only weakly coverage-dependent [29]. In a first approximation, therefore only the hydrogen adsorption enthalpy was assumed to differ from the ab initio zero coverage value.

Parameter estimation was performed using a combination of a Rosenbrock algorithm [30] and a Marquardt algorithm [31]. An in-house written code was used for the Rosenbrock method, whereas for the Marquardt algorithm, the ordinary least squares option of the ODRPACK-package version 2.01 [32] was used. The sum of squared residuals between the observed and calculated outlet flow rates of methylcyclohexane was minimized by adjusting the model parameter b, that is, the hydrogen adsorption enthalpy, which would be expected to approach the real parameter β when the optimum was reached,

$$\mathrm{SSQ} = \sum_{j=1}^{\mathrm{nob}} \left(F_{\mathrm{mch},j} - \widehat{F}_{\mathrm{mch},j}\right)^2 \xrightarrow{b} \mathrm{Min}, \tag{1}$$

where $F_{\mathrm{mch},j}$ is the observed outlet flow rate and $\widehat{F}_{\mathrm{mch},j}$ is the calculated outlet flow rate of methylcyclohexane.

The methylcyclohexane reactor outlet flow rate is calculated by solving the nonlinear reactor equation

$$\widehat{F}_{\mathrm{mch},j} - \widehat{R}_{\mathrm{mch}}(T, p_{\mathrm{H_2}}, p_{\mathrm{toluene}})W_j = 0, \tag{2}$$

that is, via the mass balance for methylcyclohexane, where $\widehat{R}_{\mathrm{mch}}$ is the predicted rate of formation of methylcyclohexane, $p_{\mathrm{H_2}}$ and p_{toluene} are the partial pressures of hydrogen and toluene at the reactor outlet, and W_j is the catalyst mass.

The statistical significance of the global regression was expressed by means of the so-called F-test, which is based on the comparison of the calculated sum of squares and the residual sum of squares. A high F-value corresponds to a high significance of the global regression. The parameter estimate was also tested for statistical significance on the basis of its individual t-value, which is related to the sensitivity of the model calculations to the value of the parameter. A high t-value corresponds to a high sensitivity and hence to a high significance or a narrow 95% approximate individual confidence interval of the corresponding parameter.

3. Results

3.1. Rate equation

The results from the ab initio reaction path analysis [1] were used to construct a classical analytical LHHW rate expression that is easy to implement and interpret. We want to stress that the main purpose of this paper is to demonstrate the applicability of first-principles calculations in constructing a kinetic model for industrial catalytic reactions involving more complex reactants, such as toluene. The main purposes of the LHHW model presented here are to assess the validity of the assumptions derived from the ab initio reaction path analysis and to test the relative accuracy of the ab initio parameters and their suitability for modeling laboratory kinetics. Because of the simplifications introduced by the model assumptions in the LHHW model, we do not expect the model to quantitatively reproduce the experimental data; however, we hope that the model can reliably simulate the main trends. More detailed microkinetic modeling [33] or kinetic Monte-Carlo simulations [4,5] could further improve the model's accuracy, but are more difficult to construct and interpret. However, they are a logical extension if the LHHW model successfully reproduces the experimentally observed trends.

The LHHW model described here is based on five model assumptions, derived from the conclusions of the ab initio reaction path analysis [1].

Assumption 1. Competition between the dissociative adsorption of H_2 and the molecular chemisorption of the toluene for identical sites. Although benzene was found to adsorb at both the bridge and the hollow site, only hollow site adsorption was considered in the kinetic model, because it was found to be the more reactive species [1,21]. Moreover, at the high coverages observed under industrial conditions, experimental data indicate that hollow site adsorption is preferred [17]. Hydrogen and toluene are assumed to compete for the same active sites. The larger size of toluene is taken into account via the pre-exponential factor of the adsorption equilibrium coefficient. The chemisorption of both hydrogen and toluene is assumed to be quasi-equilibrated. Some kinetic models reported in the literature assume noncompetitive adsorption of hydrogen and aromatics [9–11,14,15]. Experimental work by Mirodatos [34] seems to provide support for this assumption. Using H_2 titration, Mirodatos showed that the total amount of adsorbed hydrogen does not change much with the presence of benzene on Ni. However, as argued by Toulhoat and Raybaud [35], benzene chemisorbs flat on the surface and competitive adsorption implies that the adsorption of H could locally prevent the adsorption of benzene, and vice versa. Lutterloh et al. [36] studied the coadsorption of hydrogen and benzene on Pt(111) using thermal desorption and vibrational spectroscopy. Their results provide further support that benzene and hydrogen adsorb competitively.

Assumption 2. Desorption of the hydrogenated product is fast and irreversible. The calculated adsorption enthalpy of cyclohexane is −27 kJ/mol [1,20]. Although reported experimental values are somewhat higher, at around −58 kJ/mol [37], desorption can still be assumed to be fast and irreversible, because the experimental value is still low compared with the adsorption energy of benzene, −71 kJ/mol, and the activation energy of the RDS, 104 kJ/mol.

Assumption 3. Hydrogenation follows a single reaction path where the addition of the fifth hydrogen is the RDS. This assumption follows directly from the ab initio reaction path analysis [1] summarized in Fig. 1.

Assumption 4. The lower activation barriers for steps 1–4 suggest that they can be assumed to be quasi-equilibrated. The calculated activation energies for the first three benzene hydrogenation steps are ∼75 kJ/mol, and the barrier of the fourth hydrogen addition amounts to 88 kJ/mol. The barriers for the

corresponding reverse dehydrogenation reactions are all lower than 64 kJ/mol [1,21]. The barrier for the RDS is 104 kJ/mol, which is at least 16 kJ/mol higher than for the barriers for the first four steps. At 450 K, a typical temperature for aromatic hydrogenation, such a difference in activation energies corresponds to an 80-fold difference in the reaction rate coefficient. In addition, the surface coverage of the AH_4^* reaction intermediate is likely to be lower than the surface coverage of hydrogen, toluene, or the less hydrogenated intermediates because of the endothermicity of the hydrogenation reactions. The lower coverage further limits the hydrogenation rate of the fifth step. The first four hydrogen additions can therefore be assumed to be quasi-equilibrated. The sixth hydrogenation step has a sizeable barrier of 96 kJ/mol [1] for the reverse dehydrogenation reaction. Thus this step may not be quasi-equilibrated. However, the lower hydrogenation barrier of 87 kJ/mol, along with the fact that cyclohexane desorption is irreversible (Assumption 2), indicate that the dehydrogenation reaction is not kinetically significant.

Assumption 5. Chemisorbed hydrogen and toluene are the MARIs [22]. The energy profile along the dominant reaction path is sketched in Fig. 2. The solid line corresponds to the ab initio energy profile based on the ab initio hydrogen adsorption enthalpy of −94 kJ/mol. As discussed previously, the hydrogen adsorption enthalpy decreases significantly at higher coverages. For a monolayer coverage, adsorption enthalpies as low as −40 kJ/mol have been reported [28]. A lower hydrogen adsorption enthalpy also reduces the endothermicity of the hydrogenation reactions as one hydrogen atom is consumed in each step. The dotted line in Fig. 2 corresponds to a hydrogen adsorption enthalpy of −45 kJ/mol. For such low hydrogen adsorption enthalpies, the hydrogenation reactions are nearly thermoneutral. Under industrial conditions, an intermediate value can be expected, and the hydrogenation can still be expected to be endothermic. Therefore, the thermodynamic sink of the energy profile is likely to be adsorbed toluene and hydrogen, and thus these are considered the MARIs. All other intermediates can then be neglected in the overall site balance.

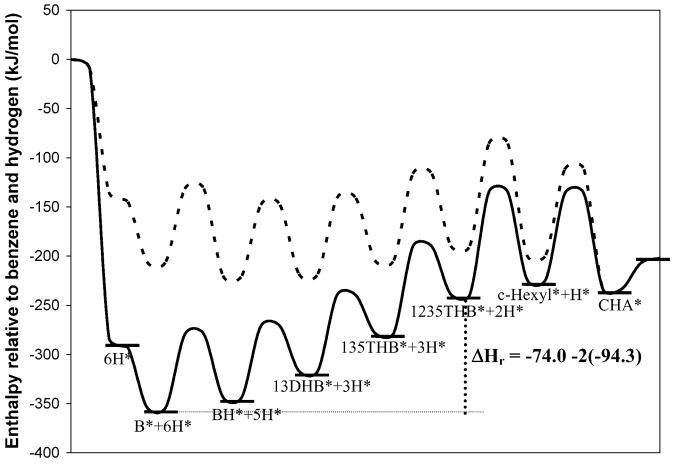

Fig. 2. DFT calculated energy profile along the dominant reaction path in Fig. 1 (—, $\Delta H_{ads}(H_2) = 94.3$ kJ/mol; - - -, $\Delta H_{ads}(H_2) = 45.0$ kJ/mol).

Assumptions 1–5 lead to the following sequence of elementary steps, using standard notation [22]:

$$
\begin{aligned}
&H_2(g) + 2^* \rightleftharpoons 2H^* && K_{H_2},\\
&A(g) + {}^* \rightleftharpoons A^* && K_A,\\
&A^* + H^* \rightleftharpoons AH^* + {}^* && K_1,\\
&AH^* + H^* \rightleftharpoons AH_2^* + {}^* && K_2,\\
&AH_2^* + H^* \rightleftharpoons AH_3^* + {}^* && K_3,\\
&AH_3^* + H^* \rightleftharpoons AH_4^* + {}^* && K_4,\\
&AH_4^* + H^* \rightarrow AH_5^* + {}^* && k_5,\\
&AH_5^* + H^* \rightarrow AH_6^* + {}^*,\\
&AH_6^* \rightarrow AH_6(g) + {}^*.
\end{aligned}
$$

With Assumptions 2 and 3, the rate of formation of the hydrogenated product, AH_6, can be written as

$$R_{AH_6(g)} = C_t k_5 \theta_{AH_4^*} \theta_{H^*} \tag{3}$$

where θ_X is the surface coverage of X, k_5 is the reaction rate coefficient for the RDS, and C_t is the surface concentration of active sites (mol kg_{cat}^{-1}).

The surface coverage of hydrogen (H^*) and aromatic (A^*) can be obtained from Assumption 1 as

$$\theta_{A^*} = \theta_* K_A p_A \quad \text{and} \quad \theta_{H^*} = \theta_* \sqrt{K_{H_2} p_{H_2}}, \tag{4}$$

where K_X is the chemisorption coefficient for X, p_X is the partial pressure, and θ_* is the surface concentration of empty sites. The surface coverage of the hydrogenated intermediates can be obtained from the quasi-equilibrium (Assumption 4) as

$$\theta_{AH_i^*} = \left(\prod_{j=1}^{i} K_j\right) \frac{\theta_{A^*} \theta_{H^*}^i}{\theta_*^i}, \quad i = 1, \ldots, 4. \tag{5}$$

This leads to the following rate equation:

$$R_{AH_6(g)} = C_t k_5 \left(\prod_{i=1}^{4} K_i\right) K_A p_A \left(\sqrt{K_{H_2} p_{H_2}}\right)^5 \theta_*^2. \tag{6}$$

A site balance is used to eliminate θ_* from the rate equation (Assumption 5),

$$1 = \theta_* + \theta_{A^*} + \theta_{H^*}, \quad \theta_* = \frac{1}{1 + K_A p_A + \sqrt{K_{H_2} p_{H_2}}}. \tag{7}$$

This leads to the following LHHW rate equation:

$$R_{AH_6(g)} = \frac{C_t k_5 \left(\prod_{j=1}^{4} K_j\right) K_A K_{H_2}^{5/2} p_A p_{H_2}^{5/2}}{(1 + K_A p_A + \sqrt{K_{H_2} p_{H_2}})^2}. \tag{8}$$

This rate equation differs from the rate equations proposed previously by Thybaut et al. [16], which were based on a reaction enthalpy diagram including only adsorbed benzene, cyclohexadiene, cyclohexene, and cyclohexane. Because the hydrogenation from cyclohexene to cyclohexane was found to be exothermic, the rate-limiting step was assumed to be the third or fourth hydrogenation step. Alternatively, a model with equal reaction rate coefficients for steps 1–4 was proposed. In all three models,

the remaining hydrogenation steps are assumed to be quasi-equilibrated. A more detailed ab initio reaction path analysis [1] provides additional insight, leading to the slightly different LHHW model equation (8).

3.2. Kinetic and thermodynamic parameters

A number of parameters appear in the LHHW rate equation (8): the concentration of active sites, C_t; the reaction rate coefficient of the RDS, k_5; the product of the equilibrium coefficients for the surface reactions, $\prod_{i=1}^{4} K_i$; and the adsorption coefficients for toluene, K_A, and hydrogen, K_{H_2}. Taking into account the temperature dependence of the rate coefficients and the adsorption coefficients, nine parameters must be determined. The concentration of active sites, C_t, must be determined experimentally, because it depends on the catalyst preparation procedure and amounts to 0.8×10^{-2} mol kg_{cat}^{-1}. The kinetic and thermodynamic parameters can be obtained from a combination of DFT calculations and statistical mechanics. We explain step by step how these parameters were derived. For the calculation of the pre-exponential factors, some additional assumptions concerning the mobility of the adsorbed molecules are required. First, the calculation of the adsorption coefficients is discussed.

The pre-exponential factors, A_{ads}, are derived from statistical mechanics (e.g., [33]),

$$A_{ads} = \frac{Q_{translation,ads}\, Q_{rotation,ads}\, Q_{vibration,ads}}{Q_{translation,gas}\, Q_{rotation,gas}\, Q_{vibration,gas}}, \qquad (9)$$

where $Q_{translation}$ is the translational partition function, $Q_{rotation}$ is the rotational partition function, and $Q_{vibration}$ is the vibrational partition function. These partition functions can be calculated from the DFT geometries, vibrational frequencies, and diffusion barriers using standard formulas (e.g., [33]). The following translational partition functions per degree of freedom (DOF) are calculated:

Toluene: $Q_{translation,DOF}\ (450\ K) = 1.17 \times 10^{11}\ m^{-1}$;

Hydrogen (H_2): $Q_{translation,DOF}\ (450\ K) = 1.72 \times 10^{10}\ m^{-1}$;

Hydrogen atom (H):

$Q_{translation,DOF}\ (450\ K) = 1.22 \times 10^{10}\ m^{-1}$.

The rotational partition functions are calculated using the ab initio gas phase geometries, where σ is the rotational symmetry number:

Toluene: $Q_{rotation,DOF}\ (450\ K) = 25.1\ (\sigma = 2);\ 74.4; 89.2$ for the three rotational axes;

Hydrogen (H_2): $Q_{rotation}\ (450\ K) = 2.59\ (\sigma = 2)$.

For wave numbers larger than 700 cm^{-1}, the vibrational partition functions are ∼1. From Eq. (9), the pre-exponential factors can be calculated.

3.3. Adsorbed toluene

The DFT calculations indicate that benzene adsorbed at the hollow site is fairly mobile, with a diffusion barrier of ∼5 kJ/mol [17]. A similar mobility can be assumed for toluene. The translational partition function for the chemisorbed toluene is therefore approximated as $(Q_{translation,DOF})^2$. Chemisorbed toluene is also assumed to retain 1 rotational DOF, that is, $Q_{rotation,DOF} = 89.2$. The vibrational partition function of adsorbed toluene can be written as $Q_{vib,gas} Q_{vib,extra}$, where $Q_{vib,extra}$ accounts for the low-frequency C–Pt stretch frequencies that appear on adsorption. For benzene, C–Pt stretch frequencies of ∼300 cm^{-1} were calculated [17,18], leading to a $Q_{vib,extra}$ of about 10. As usual, the translational partition functions are multiplied with the space available for the molecule, that is, the surface area available to a single molecule and the volume available to the molecule [33]. These considerations lead to the following pre-exponential factor for the adsorption coefficient:

$$A_{ads,A} = \frac{(1.17 \times 10^{11})^2 \times 89.2\, Q_{vib,ads}\ (m^{-2}) \times 1 \times 10^{-18}\ (m^2)}{(1.17 \times 10^{11})^3 \times 89.2 \times 25.1 \times 74.4\, Q_{vib,gas}\ (m^{-3}) \times kT\ (Pa\,m^3)} = 7.4 \times 10^{-12}\ Pa^{-1},$$

where a surface area per adsorbed toluene of 10×10^{-19} m^2 is assumed, consistent with a value of 5×10^{-19} m^2 that has been determined experimentally for benzene [38] and with the value that can be calculated from the van der Waals radii for toluene (i.e., 4.8×10^{-19} m^2). A typical surface area per platinum atom is 10^{-19} m^2. The DFT adsorption enthalpy of benzene at the hollow site, −71 kJ/mol, was taken as the chemisorption enthalpy for toluene. To validate the assumption that the toluene adsorption energy is similar to the value for benzene, the toluene adsorption energy was treated as an adjustable parameter, in addition to the hydrogen adsorption energy. The estimated value, -69.6 ± 2.0 kJ/mol, indeed indicates that the toluene adsorption energy does not differ significantly from the ab initio value for benzene. Thus in the final model we will use the ab initio value, rather than the estimated value.

3.4. Adsorbed hydrogen

Hydrogen is found to be highly mobile on the Pt(111) surface as well, with a barrier of < 5 kJ/mol for diffusion (e.g., [21]). For hydrogen adsorption, the pre-exponential factor can thus be calculated in a similar way,

$$A_{H_2} = \frac{[(1.22 \times 10^{10})^2]^2 \times [10^{-19}]^2}{(1.72 \times 10^{10})^3 \times 2.59kT} = 2.7 \times 10^{-9}\ Pa^{-1}.$$

Differential enthalpy diagrams of hydrogen adsorption show that the adsorption enthalpy decreases from about −90 kJ/mol at low coverage to about −40 kJ/mol at near-monolayer coverage. Instead of assigning the low-coverage DFT value of −94 kJ/mol, we thus treat the hydrogen adsorption enthalpy as an adjustable parameter, $\Delta H_{ads}(H_2)$.

3.5. Equilibrium coefficient

The changes in the hydrogen adsorption enthalpy also affect the reaction enthalpy of the elementary hydrogenation steps.

To illustrate this effect, the energy profile for a hydrogen adsorption energy of −45 kJ/mol is shown in Fig. 2 (dotted line). The reaction enthalpies of the individual steps, $\Delta H_{r,i}$, are therefore functions of the hydrogen adsorption enthalpy, $\Delta H_{ads}(H_2)$. Note that in Fig. 2 the simplifying assumption has been made that the hydrogenation barriers are unaffected by the value of the hydrogen adsorption energies. The lower H–Pt binding energy could result in a lowering of the hydrogenation activation energies as well.

The reaction enthalpy for the product of the equilibrium constants, $\prod_{i=1}^{4} K_i$, can be determined from the ab initio enthalpy diagram,

$$\sum_{i=1}^{4} \Delta H_{r,i} = \Delta H_f(1235\text{THB,g}) - \Delta H_f(\text{B,g}) + \Delta H_{ads}(1235\text{THB}) - \Delta H_{ads}(\text{B}) - 2\Delta H_{ads}(H_2),$$

$$\sum_{i=1}^{4} \Delta H_{r,i} = -74\ \text{kJ/mol} - 2\Delta H_{ads}(H_2),$$

where ΔH_f(1235THB,g) is the gas phase enthalpy of formation of 1,2,3,5-tetrahydrobenzene and ΔH_{ads}(1235THB) is the corresponding adsorption enthalpy. ΔH_f(1235THB,g) is calculated using the atom additivity-corrected CBS-QB3 method [25] and amounts to 271 kJ/mol. ΔH_{ads}(1235THB) was obtained from a cluster DFT calculation and equals −333 kJ/mol. ΔH_f(B,g) is the gas phase enthalpy of formation of benzene, 83 kJ/mol [39], and ΔH_{ads}(B) is the DFT adsorption enthalpy for the hollow site, −71 kJ/mol. The adsorption energy of benzene rather than that of toluene is used, to be consistent with the adsorption energy and the enthalpy of formation for 1235THB.

The determination of the pre-exponential factors for the surface reaction equilibrium coefficient requires some approximations, because the diffusion barriers of the hydrogenated intermediates have not been explicitly calculated nor measured. Hence it is not possible to calculate the partition functions from statistical mechanics using the first principles data as we did for adsorbed hydrogen and toluene. Instead, the pre-exponential factors are determined by combining the DFT structures with experimental surface science data.

Typical values for the pre-exponential factor of a dehydrogenation rate coefficient for cyclic C_6 molecules can be found in the surface science literature [40]. For cyclohexane on Pt(111), a pre-exponential factor of 3×10^{12} s^{-1} has been determined. For cyclohexene on Pt(111), a value of 6×10^{11} s^{-1} has been reported. Here we assume an intermediate value of 1×10^{12} s^{-1} for the pre-exponential factor for the dehydrogenation reactions. The hydrogenation pre-exponential factor can now be estimated from statistical thermodynamics. Adsorbed hydrogen is found to be mobile, whereas the adsorbed hydrogenated intermediates are assumed to be less mobile because they are bound by rather strong σ_{C-Pt} bonds. For the transition state, an intermediate mobility can be assumed. This leads to pre-exponential factors between 10^{11} and 10^{12} s^{-1} [33]. During hydrogenation, a mobile (H^*) and a less-mobile reactant are converted to a less-mobile product, leading to a negative reaction entropy. Therefore, the hydrogenation pre-exponential factor must be smaller than the dehydrogenation value, 10^{12} s^{-1}. A reasonable estimate for the hydrogenation pre-exponential factor is therefore 5×10^{11} s^{-1}. Hence the pre-exponential factor for the surface reaction equilibrium coefficient equals $(0.5)^4 = 0.06$.

Table 1
First principle derived kinetic and thermodynamic parameters to be used in the LHHW rate equation (8)

Parameter	Pre-exponential factor	Enthalpy/activation energy (kJ/mol)
C_t	0.8×10^{-2} mol/kg$_{cat}$	–
k_5	5×10^{11} s^{-1}	104
$\prod_{i=1}^{4} K_i$	$(0.5)^4 = 0.06$	$-74 - 2\Delta H_{ads}(H_2)$
K_A	7.4×10^{-12} Pa^{-1}	−71
K_{H_2}	2.7×10^{-9} Pa^{-1}	$\Delta H_{ads}(H_2)$

3.6. Rate-determining step

In the previous section, a pre-exponential factor of 5×10^{11} s^{-1} was proposed for hydrogenation reactions. The same value is used for the pre-exponential factor of the RDS, A_5. The pre-exponential factor for the RDS and the pre-exponential factor for the equilibrium coefficient are taken from experimental surface science data, in combination with qualitative arguments based on the ab initio geometries and surface mobilities. This introduces some experimental data into our ab initio model. Calculating these parameters from first principles would be possible, yet very time-consuming. To validate the proposed parameters, we have estimated the pre-exponential factor for the parameter combination $k_5(\prod_{j=1}^{4} K_j)$ [Eq. (8)]. The estimated value does not differ significantly from the calculated value, and we use the latter in our model. For the RDS, an activation energy of 104 kJ/mol is calculated (Fig. 2). Note that for less negative hydrogen adsorption enthalpies, a slightly lower value could be expected.

Table 1 summarizes the parameters required in the LHHW rate equation (8). The pre-exponential factors presented here differ slightly from the values reported previously [16]. Therein the mobility was assumed to be low for the adsorbed toluene, whereas new insights from the DFT calculations indicate the aromatic reactant is highly mobile. In addition, for the hydrogen atoms a lower mobility was assumed in previous work.

4. Discussion and comparison with kinetic data

The rate equation (8) was implemented in a CSTR reactor model for the simulation of lab-scale data for the hydrogenation of toluene on Pt/ZSM-22. The hydrogen adsorption enthalpy, $\Delta H_{ads}(H_2)$, which is known to be strongly coverage-dependent, was optimized to fit the experimental data. A hydrogen adsorption enthalpy, $\Delta H_{ads}(H_2)$, of -54.0 ± 1.0 kJ/mol was determined. The kinetic model was found to be statistically significant, with a calculated F-value of 1070. The model predictions were compared with the experimental data in a parity diagram (Fig. 3). The first-principles based kinetic model clearly captures the main trends in the reaction rate. The es-

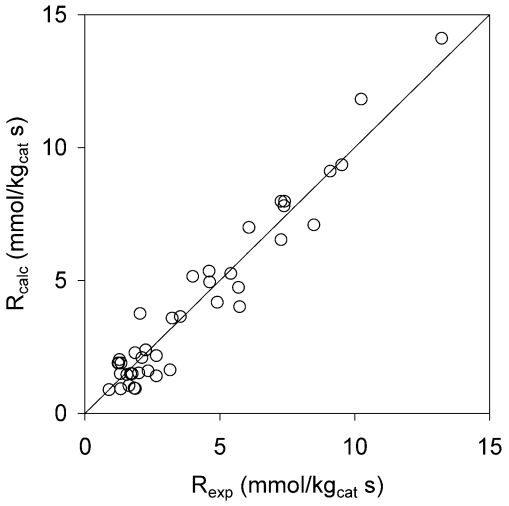

Fig. 3. Parity diagram for the methylcyclohexane outlet flow rate (line, experimental; dots, calculated based on kinetic model equation (Eq. (8)) and parameters from Table 1).

Table 2
Partial reaction orders in H_2 and toluene inlet partial pressure for the different experimental temperatures. Comparison between experimental [16] and simulated values

T	Hydrogen		Toluene	
(K)	Experimental	Simulated[a]	Experimental	Simulated[a]
423	0.6 ± 0.1	1.7 to 2.4	-0.2 ± 0.1	-0.7 to $+0.5$
448	1.1 ± 0.05	1.6 to 2.3	-0.2 ± 0.1	-0.5 to $+0.7$
473	1.8 ± 0.05	1.6 to 2.2	-0.1 ± 0.05	-0.2 to $+0.8$
498	1.3 ± 0.05	1.6 to 2.0	$+0.3 \pm 0.1$	0.0 to $+0.9$

[a] Values indicate range of partial reaction orders that can be calculated for the range of experimental process conditions.

timated hydrogen adsorption enthalpy is intermediate between the low coverage value of about -90 kJ/mol and the monolayer value of about -45 kJ/mol, consistent with simulated hydrogen coverages for the experimental data varying from 31 to 82%, with an average value of 61%. The estimated hydrogen adsorption enthalpy is likely an average value, and more detailed models will need to take into account the variation of the hydrogen adsorption enthalpy with coverage.

Next we present a more detailed discussion of the simulated trends versus hydrogen and toluene partial pressure, temperature, and space–time. The partial reaction order in hydrogen partial pressure is determined mainly by the location of the RDS, whereas the partial reaction order in the aromatic reactant is related largely to the hypotheses of competitive adsorption and the presence of a rate-determining reaction step. The variation of the reaction rate with temperature and the position of the maximum in the reaction rate–temperature curve are related primarily to the relative values of the kinetic and thermodynamic parameters. The simulated variation of the reaction rate with space–time can provide an indication of the overall reliability of the first-principles based reaction model.

Table 2 lists the partial reaction orders in the hydrogen and toluene inlet partial pressures for different temperatures. The experimental partial reaction orders were determined by regression of all experimental data at a given temperature to Eq. (10),

$$R_{AH_6(g)} = k_{AH_6(g)}\, p_{tol,in}^{m}\, p_{H_2,in}^{n}. \tag{10}$$

Note that the reaction orders relate the *inlet* partial pressures (set values) to the reaction rate. But the LHHW model relates the partial pressures inside the reactor to the reaction rate. The reactor model equations in turn relate the reactor partial pressures to the inlet partial pressures.

For the LHHW rate equation (8), the reaction order in the hydrogen reactor partial pressure can be obtained analytically as

$$\text{reaction order in } p_{H_2} = \frac{5}{2} - \frac{\sqrt{K_{H_2} p_{H_2}}}{1 + K_A p_A + \sqrt{K_{H_2} p_{H_2}}} \tag{11}$$

and can vary between 1.5 and 2.5. However, the ab initio partial reaction orders must be calculated from CSTR reactor simulations for the different process conditions. Over the range of experimental conditions, the ab initio model yields partial reaction orders in *inlet* hydrogen partial pressure ranging from 1.6 to 2.4 (Table 2). Note that the range in the simulated partial reaction orders at any temperature is quite large, and hence the partial reaction orders are strongly dependent on the conditions at which the experiments were carried out. At 473 K, the temperature at which most of the experiments were carried out, the experimental reaction order is in the simulated range. At lower temperatures, the agreement is less satisfactory, and the LHHW model overestimates the experimental reaction orders. One reason for this might be that the experiments at lower temperatures were done over a limited range of partial pressures and correspond to the lower range of the simulated reaction orders. Moreover, the higher coverages at lower temperature might require a lower value for the adsorption enthalpies. From Eq. (11), it follows that the hydrogen partial reaction order is rather sensitive to adsorption energy of the aromatic reactant. Indeed, increasing the toluene adsorption energy from -70.6 to -60.6 kJ/mol leads to a decrease in reaction order of 0.2–0.5. Note that a lower toluene adsorption enthalpy might be expected, because the ab initio value corresponds to low coverages, whereas the simulated surface coverages are rather high. As discussed, the reaction order in hydrogen partial pressure is mostly determined by the location of the RDS. The fair agreement in Table 2, particularly for the data at 473 K, where most of the experiments were performed, gives some validation to the location of the RDS based on the ab initio reaction path analysis.

For the aromatic reactant, partial reaction orders between -1 and $+1$ have been reported in the literature [9–16], depending on the experimental conditions. In the experimental studies discussed here, the range of observed reaction orders is much smaller, from -0.2 to 0.3 (Table 2). At lower temperatures, the reaction order tends to be negative, whereas at higher temperatures it becomes slightly positive. For the LHHW rate equation (8), the partial reaction order in toluene is given by

$$\text{reaction order in } p_A = 1 - \frac{2K_A p_A}{1 + K_A p_A + \sqrt{K_{H_2} p_{H_2}}} \tag{12}$$

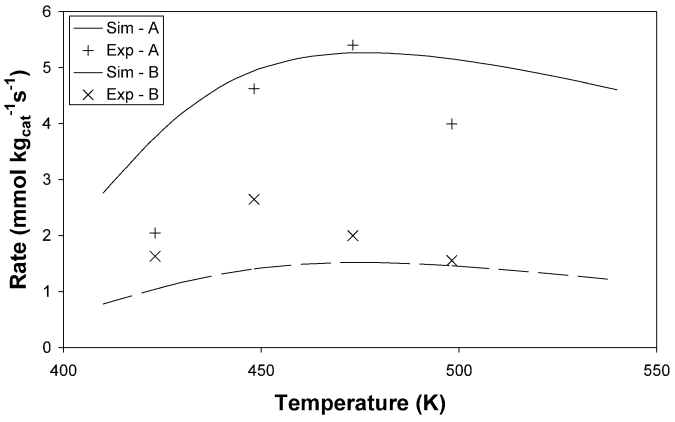

Fig. 4. Plot of the reaction rate versus temperature. Reaction conditions: $p_{\text{total}} = 10$ bar; $W/F_{\text{tol},0} = 81.8\ \text{kg}_{\text{cat}}\,\text{s}\,\text{mol}^{-1}$; $p_{\text{toluene},0} = 20.3$ kPa (A), 10.1 kPa (B); $p_{\text{H}_2,0} = 202$ kPa (A), 101 kPa (B).

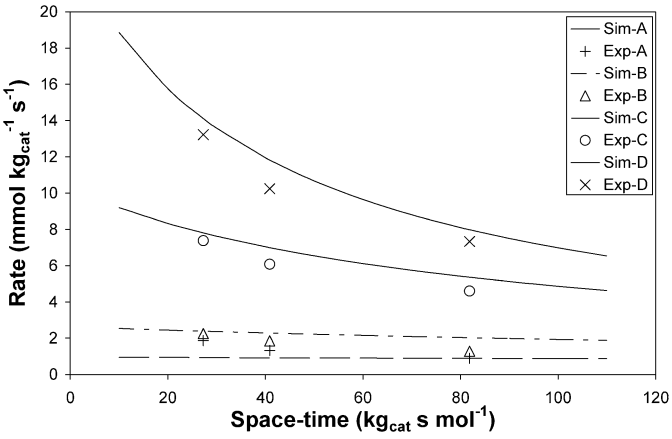

Fig. 5. Plot of the reaction rate versus space–time. Reaction conditions: $p_{\text{total}} = 10$ bar (A, B), 20 bar (C), 30 bar (D); $T = 423$ K (A), 498 K (B), 473 K (C, D); $p_{\text{H}_2,0} = 101$ kPa (A, B), 203 kPa (C), 304 kPa (D); $p_{\text{toluene},0} = 20.3$ kPa (A, B), 40.5 kPa (C), 60.8 kPa (D).

and ranges from -1 to $+1$. Because K_{A} decreases with temperature, the predicted reaction order increases with temperature, as has been found experimentally. Over the range of experimental data, the ab initio kinetic model predicts partial reaction orders ranging from -0.7 to 0.9 and increasing with temperature, in fair agreement with the experimental values (Table 2).

Fig. 4 plots the reaction rate versus temperature. Both the ab initio model and the experimental data clearly show a maximum in rate versus temperature; however, the change in the ab initio predicted rate with temperature is smaller than the experimental variations, and the predicted maximum is at slightly higher temperatures for the lower reactant partial pressures. The position of the maximum and the steepness of the curve are determined by $\text{d}R_{\text{AH}_6(\text{g})}/\text{d}T$, as follows:

$$\frac{\text{d}R_{\text{AH}_6(\text{g})}}{\text{d}T} = \frac{R_{\text{AH}_6(\text{g})}}{RT^2} \times \left[E_{\text{a},5} + \sum_{i=1}^{4} \Delta H_{\text{r},i} + \Delta H_{\text{ads}}(\text{A}) + 2.5\Delta H_{\text{ads}}(\text{H}_2) - \frac{2\Delta H_{\text{ads}}(\text{A}) K_{\text{A}} p_{\text{A}} + \Delta H_{\text{ads}}(\text{H}_2)\sqrt{K_{\text{H}_2} p_{\text{H}_2}}}{1 + K_{\text{A}} p_{\text{A}} + \sqrt{K_{\text{H}_2} p_{\text{H}_2}}} \right]. \quad (13)$$

The sum $E_{\text{a},5} + \sum_{i=1}^{4} \Delta H_{\text{r},i} + \Delta H_{\text{ads}}(\text{A}) + 2.5\Delta H_{\text{ads}}(\text{H}_2)$ is negative for the parameters determined here, and the fraction is always negative. Decreasing the activation energy of the RDS, $E_{\text{a},5}$, shifts the maximum to lower temperatures, and the profile also becomes steeper. This improves the agreement with the experimental trend. Note that lower hydrogenation activation energy can indeed be expected for lower hydrogen adsorption enthalpies. A less endothermic reaction enthalpy, $\sum_{i=1}^{4} \Delta H_{\text{r},i}$ would have a similar effect. Indeed, for temperatures below the temperature corresponding with the maximum in the reaction rate, the rate increases with temperature because of the increase in the reaction rate coefficient, k_5, and the equilibrium coefficient, $\prod_{i=1}^{4} K_i$. The influence of the hydrogen and toluene adsorption enthalpies is less straightforward, because they appear in both terms. For the ab initio parameters and the experimental conditions reported here, decreasing the toluene adsorption enthalpy is found to shift the position of the maximum to lower temperatures because of the second part, but the effect depends on the process conditions. Taking into account the coverage dependence of the parameters will also increase the variation of the rate with temperature and might improve the agreement with the experimental data.

Fig. 5 shows the simulated and experimental variation of the reaction rate with space–time, $W/F_{\text{tol},0}$. The model accurately predicts the decrease of the rate with increasing space–time, particularly for higher reaction rates. At lower rates, the predicted variations are somewhat smaller than the experimentally observed variations.

In general, the first-principles based LHHW model rather accurately simulates the trends of the experimental data. To further improve the agreement, some of the assumptions used to determine the kinetic and thermodynamic parameters in the classical LHHW model should be refined. In particular, taking into account the coverage dependence of the hydrogen and toluene adsorption enthalpy, as well as the activation energy of the RDS, might improve the simulations. In addition, more detailed first-principles calculations of the pre-exponential factors would also likely improve the simulations.

5. Conclusions

In this work, a kinetic model for the hydrogenation of toluene over platinum catalysts was derived based on a detailed ab initio reaction path analysis for the hydrogenation of benzene over Pt(111). The kinetic and thermodynamic parameters in the model were obtained from ab initio calculations and from statistical mechanics. The first-principles based model was validated against lab-scale experimental data for the hydrogenation of toluene over a 0.5 wt% Pt/ZSM-22.

From the ab initio reaction path analysis [1], the following model assumptions were derived: (i) dissociative hydrogen and molecular toluene chemisorption are competitive, (ii) desorption of the hydrogenated product is irreversible, (iii) hydrogenation follows a single reaction path in which the addition of the fifth hydrogen is the RDS, and (iv) the hydrogen and aromatic reactants are likely the MARIs. Based on these hypotheses,

a simple LHHW kinetic model was constructed and implemented in a mathematical reactor model. The kinetic parameters in the model were obtained from the first-principles calculations, in combination with statistical mechanics, although some additional assumptions were required to derive the pre-exponential factors. The ab initio parameters corresponded to low surface coverage values. Because the hydrogen adsorption enthalpy is know to be strongly coverage-dependent, it was optimized to fit the experimental data. The resulting value, −54 kJ/mol, was found to correspond with rather high coverage values, consistent with a simulated average hydrogen surface coverage of 61%. Although the LHHW model is clearly a simplification, the main trends of the kinetics of the hydrogenation reaction are captured. More detailed microkinetic or kinetic Monte-Carlo modeling, explicitly taking into account the coverage dependence of the kinetic and thermodynamic parameters, is a logical next step. The additional parameters required in such a model can also be obtained from our DFT calculations.

This work demonstrates how detailed ab initio studies can contribute to the modeling of complex catalytic reactions in that they provide molecular level insight that extends and complements our chemical intuition. Moreover, ab initio calculations can provide reasonably accurate estimates for the kinetic and thermodynamic parameters.

Acknowledgment

M.S. is grateful to the Fund for Scientific Research-Flanders, Belgium (F.W.O.-Vlaanderen) for a research assistantship.

References

[1] M. Saeys, M.-F. Reyniers, M. Neurock, G.B. Marin, J. Phys. Chem. B 109 (2005) 2064.
[2] M. Neurock, J. Catal. 216 (2003) 73.
[3] M. Neurock, V. Pallassana, R.A. van Santen, J. Am. Chem. Soc. 122 (2000) 1150;
M. Neurock, R.A. van Santen, J. Phys. Chem. B 104 (2000) 11127.
[4] E.W. Hansen, M. Neurock, J. Catal. 196 (2000) 241.
[5] S.G. Podkolzin, R. Alcala, J.J. de Pablo, J.A. Dumesic, J. Phys. Chem. B 106 (2002) 9604.
[6] A. Logadottir, J.K. Norskov, J. Catal. 220 (2003) 273.
[7] S. Linic, M.A. Barteau, J. Catal. 214 (2003) 200.
[8] B.H. Cooper, B.B.L. Donnis, Appl. Catal. A 137 (1996) 203;
M. Schuller, P. Hodges, in: G. Emig, M. Rupp, J. Weitkamp (Eds.), Proceedings of the DGMK Conference “The Future Role of Aromatics in Refining and Petrochemistry,” Erlangen, 1999, p. 21.
[9] S.D. Lin, M.A. Vannice, J. Catal. 143 (1993) 563.
[10] M.V. Rahaman, M.A. Vannice, J. Catal. 127 (1991) 267.
[11] C. Mirodatos, J.A. Dalmon, G.A. Martin, J. Catal. 105 (1987) 405.
[12] S. Smeds, D. Murzin, T. Salmi, Appl. Catal. A 150 (1997) 115.
[13] L.P. Lindfors, T. Salmi, S. Smeds, Chem. Eng. Sci. 48 (1993) 3813.
[14] R.Z.C. Van Meerten, J.W.E. Coenen, J. Catal. 46 (1977) 13.
[15] P. Chou, M.A. Vannice, J. Catal. 107 (1987) 140.
[16] J.W. Thybaut, M. Saeys, G.B. Marin, Chem. Eng. J. 90 (2002) 117.
[17] M. Saeys, M.-F. Reyniers, G.B. Marin, M. Neurock, J. Phys. Chem. B 106 (2002) 7489.
[18] C. Morin, D. Simon, P. Sautet, J. Phys. Chem. B 108 (2004) 5653;
C. Morin, D. Simon, P. Sautet, J. Phys. Chem. B 107 (2003) 2995;
S. Yamagishi, S.J. Jenkins, D.A. King, J. Chem. Phys. 114 (2001) 5765;
F. Mittendorfer, J. Hafner, Surf. Sci. 472 (2001) 133;
F. Mittendorfer, C. Thomazeau, P. Raybaud, H. Toulhoat, J. Phys. Chem. B 107 (2003) 12287.
[19] M. Saeys, M.-F. Reyniers, G.B. Marin, M. Neurock, Surf. Sci. 513 (2002) 315.
[20] M. Saeys, PhD thesis, Ghent University, 2002.
[21] M. Saeys, M.-F. Reyniers, M. Neurock, G.B. Marin, J. Phys. Chem. B 107 (2003) 3844.
[22] M. Boudart, AIChE J. 18 (1972) 465;
M. Boudart, G. Djéga-Mariadassou, Kinetics of Heterogeneous Catalytic Reactions, Princeton University Press, Princeton, NJ, 1984;
G. Djéga-Mariadassou, M. Boudart, J. Catal. 216 (2003) 89.
[23] D. Poondi, M.A. Vannice, J. Catal. 161 (1996) 742.
[24] W. Koch, M.C. Holthausen, A Chemist’s Guide to Density Functional Theory, second ed., Wiley–VCH, Weinheim, 2001.
[25] M. Saeys, M.-F. Reyniers, G.B. Marin, V. Van Speybroeck, M. Waroquier, J. Phys. Chem. A 107 (2003) 9147.
[26] J.A. Martens, R. Parton, L. Uytterhoeven, P.A. Jacobs, G.F. Froment, Appl. Catal. 76 (1991) 95;
R. Parton, L. Uytterhoeven, J.A. Martens, P.A. Jacobs, Appl. Catal. 76 (1991) 131.
[27] J.M. Berty, Chem. Eng. Progr. 70 (1974) 78.
[28] S.G. Podkolzin, R.M. Watwe, Q. Yan, J.J. de Pablo, J.A. Dumesic, J. Phys. Chem. B 105 (2001) 8550.
[29] C. Xu, Y.-L. Tsai, B.E. Koel, J. Phys. Chem. 98 (1994) 585;
J.M. Campbell, S.G. Seimanides, C.T. Campbell, J. Phys. Chem. 93 (1989) 815.
[30] H.H. Rosenbrock, Comput. J. 3 (1960) 175.
[31] D.W. Marquardt, Ind. Appl. Math. 11 (1963) 431–439.
[32] Netlib, http://www.netlib.org.
[33] J.A. Dumesic, D.F. Rudd, L.M. Aparicio, J.E. Rekoske, A.A. Treviño, The Microkinetics of Heterogeneous Catalysis, American Chemical Society, Washington, DC, 1993.
[34] C. Mirodatos, J. Phys. Chem. 90 (1986) 481.
[35] H. Toulhoat, P. Raybaud, J. Catal. 216 (2003) 63.
[36] C. Lutterloh, J. Biener, K. Pöhlmann, A. Schenk, J. Küppers, Surf. Sci. 352–354 (1996) 133.
[37] M.E. Bussell, F.C. Henn, C.T. Campbell, J. Phys. Chem. 96 (1992) 5978;
J.A. Rodriguez, C.T. Campbell, J. Phys. Chem. 93 (1989) 826.
[38] L.T. Ngo, L. Xu, A.W. Grant, C.T. Campbell, J. Phys. Chem. B 107 (2003) 1174.
[39] H.Y. Afeefy, J.F. Liebman, S.E. Stein, Neutral Thermochemical Data, in: P.J. Linstrom, W.G. Mallard (Eds.), NIST Chemistry WebBook, NIST Standard Reference Database Number 69, National Institute of Standards and Technology, Gaithersburg, MD, 2001, http://webbook.nist-.gov.
[40] C.T. Campbell, Y.-K. Sun, W.H. Weinberg, Chem. Phys. Lett. 179 (1991) 53.